revised

SAND99-2987J

DUAL-LAYER ASYMMETRIC MICROPOROUS SILICA MEMBRANES

Chung-Yi Tsai*, Siu-Yue Tam*, Yunfeng Lu# and C. Jeffrey Brinker#

The University of New Mexico/NSF Center for Micro-Engineered Materials*,#, Sandia National Laboratories#, The Advanced Materials Laboratory, 1001 University Blvd. SE

Albuquerque, NM 87106 USA

Key words: gas separations; inorganic membranes; membrane preparation and structure; microporous and porous membranes, CO_2 removal

---

Corresponding authors, Chung-Yi Tsai (Tel: 272-7634; Fax: +505-272-7304; E-mail: cytsai@unm.edu) and C. Jeffrey Brinker (Tel: 272-7627; Fax: +505-272-7304; E-mail: cjbrink@sandia.gov)

DISCLAIMER

ABSTRACT

We report a novel sol-gel dip-coating process to form dual-layer microporous silica membranes with improved membrane performance and reproducibility. First, we deposit a surfactant-templated silica (STS) intermediate layer on top of a commercial γ–alumina support both to improve its "surface finish" and to prevent a subsequently deposited microporous overlayer from penetrating into the support. Second, membranes are processed under clean room conditions to avoid dust contamination and, third, membranes are vacuum-calcined to promote further pore shrinkage and impart surface hydrophobicity. The resulting asymmetric membrane exhibits a gradual change in pore diameter from 50Å (γ–alumina support layer) to 10-12Å (STS intermediate layer), and then to 3-4Å (30nm thick, ultramicroporous silica top-layer). Compared to a single-layer process using only the microporous overlayer, the dual-layer process improves both flux and selectivity. For the industrially important problem of natural gas purification, the combined CO_2 flux [$(3\sim0.5)\times10^{-4}$ $cm^3(STP)/(s\cdot cm^2\cdot cm\text{-}Hg)$] and CO_2/CH_4 separation factors [200~600] are superior to all previously reported values for separation of a 50/50 (v/v) CO_2/CH_4 gas mixture. In addition, the membrane selectively separated hydrogen from a simulated reformate from partial oxidation of methanol as evidenced by a high concentration of hydrogen recovery.

1. INTRODUCTION

Membrane-based separations are energy efficient and cost effective. They represent promising alternatives to energy-intensive distillation, cryogenic separation, or pressure swing adsorption in applications such as purification of sub-quality natural gas, air separation, removal of VOCs and NO_X, and hydrogen recovery from processing gases and feed stocks [1,2]. Microporous inorganic membranes have attracted considerable attention for gas separation due to their excellent thermal and chemical stability, good erosion resistance and high-pressure stability compared to conventional polymeric membranes (e.g. cellulosic derivatives, polysulfone, polyamide, or polyimide membrane).

An inorganic membrane system generally consists of a macroporous support providing mechanical strength for an overlying thin, either dense or porous, separation membrane. Dense membranes prepared from palladium or perovskite only allow certain gases (such as H_2 or O_2) to transport via mechanisms such as solution-diffusion or solid-state ionic conduction. Such membranes require high capital investment due to the use of precious metals and/or extreme synthesis conditions [3,4]. In contrast, porous silica membranes with tunable pore sizes can be processed by a simple dip-coating or spin-coating procedure and can be used potentially in a large variety of gas separations [5]. Microporous silica membranes have been demonstrated to show promising molecular sieving characteristics by several research groups [6,7,8,9]; however, the improvement of membrane performance (flux and selectivity), processibility, and stability remains a challenge.

Several techniques have been developed to process porous silica membranes. They include sol-gel synthesis [10,11], leaching [12], and chemical vapor deposition [13]. Among these, sol-gel processing attracts most attention due to its excellent processibility and its potential to precisely control pore size and pore structure [6]. Brinker et al. have proposed several strategies for the fundamental physical and chemical phenomena involved in the deposition of colloidal ceramic dispersions (sols) on porous supports for precise pore size and porosity control. Three keys to membrane production are 1) avoidance of cracks, pinholes, or other defects that would reduce the selectivity; 2) precise pore size control (0.3 - 0.4 nm in diameter) so that separation occurs on the basis of size by molecular filtration or "sieving"; and 3) maximization of the volume fraction porosity and minimization of the membrane thickness to maximize flux [6].

Recently, De Vos and Verweij synthesized a sol-gel derived microporous silica membrane on top of a home-made, disk-shaped, γ-alumina support [9]. They applied both repeated-coating and processing under clean room conditions to reduce membrane defects. In general, the multi-step coating process would aid in reduction of the number of defect sites, thus increasing selectivity, but at the expense of permeation flux by adding flow resistance [14]. Although high selectivity can significantly reduce either feed loss (single stage) or recompression costs (multiple stage), high permeation flux is necessary to achieve commercially satisfactory production rates. Therefore, both high selectivity and high flux are equally important in real-world membrane applications.

It has been known that the quality of the underlying support determines, to a high degree, the properties and quality of the top selective microporous silica membrane. Rough or large-pore support surfaces would cause cracking of overlying sol-gel derived membranes due to stress development on uneven film coatings [11]. Therefore, it is important to develop a simple and effective way to modify the support surface to facilitate deposition of a defect-free overlying microporous membrane. Conventional mechanical-polishing requires tedious, repetitious steps to remove surface roughness and is impractical for polishing the interiors of tubular supports. Alternatively, in the present study, we modify the interior surface of a tubular, asymmetric, γ-alumina membrane support with a layer of *surfactant-templated porous silica* (STS) via a dip-coating process. The STS with high porosity and narrow pore size distribution (1-2 nm) is designed to minimize flow resistance, surface roughness, and inherent support defects. It also prevents subsequently deposited silica sol from penetrating further into the support, thus forming a very thin overlying microporous selective layer. Compared to a single-layer process using only the microporous overlayer, the dual-layer process should improve *both* flux (due to thinner effective separation layer) and selectivity (due to less defects).

In the present study, we first address the problem of CO_2/CH_4 separation and then extend the same separation principle to H_2 purification for fuel-cell applications and NO removal from power-plant exhaust gas. For comparison to other literature data, besides single-gas permeation measurements, mixed-gas permeation measurements are also

performed both for separation of CO_2 from a 50/50 (v/v) CO_2/CH_4 gas mixture and for H_2 separation from a simulated reformate gas under low-temperature conditions. Permeate-side sweeping gases commonly used in laboratory practice are impractical in industrial applications. They either increase energy consumption required for both pumping and downstream separation or cause back-diffusion resulting in dilution of the feed stream. Sweeping gas is thus not used in our permeation experiments. Moreover, a new processing condition is developed to improve long-term stability of the membranes. The influence of a number of operating parameters (temperature, pressure gradient across the membrane, and feed flow rates) for a tube-and-shell configuration membrane separator is elucidated.

2. MATERIALS AND EXPERIMENTAL

Silica sol preparation

All silica membranes of the present study were prepared from an A2** sol. Preparation of the A2** sol consists of two acid-catalyzed reaction steps designed to minimize the condensation rates of silica species in order to produce weakly branched polymeric clusters that maximize interpenetration and collapse during film deposition to produce membranes with molecular-sized pores [15]. In the first step, the A2** *stock sol* with TEOS: EtOH: H_2O: HCl = 1.0: 3.8: 1.1: 5×10^{-5} (pH = 4.7) was prepared by refluxing the sol for 90 minutes at 60°C. The sol can then be stored in a -30°C freezer. In the second step, additional water and HCl were added to the stock sol. The sol was

agitated for 15 minutes prior to aging at 50°C for 22 hours. The two-step procedure resulted in a *standard sol* with a final molar ratio of TEOS: EtOH: H_2O: HCl = 1.0: 3.8: 5.0: 0.004 (ca. pH = 2.0). A dip-coating sol was prepared by diluting the *standard sol* with two times its volume of ethanol. Moreover, a 0.125M C6-surfactant (triethylhexylammonium bromide, Aldrich) or a 4.2wt% C16-surfactant (cetyltrimethylammonium bromide, Aldrich) silica sol was prepared by adding a corresponding amount of surfactant powder into the unaged A2** standard sol prior to diluting the *sol* with two times its volume of ethanol. The aggregation of the surfactants during membrane drying did not cause any phase separation. All sols were filtered through a 0.45μm filter (Nalgene) prior to coating.

Membrane preparation

Membrane supports were prepared by sectioning a commercial 50Å γ-Al_2O_3 tube (ID=0.7cm, OD=1cm, US Filter) into 5.5 cm-long sections cleaned subsequently by ultrasound. The supports were then washed with de-ionized water several times prior to calcining at 400°C for one hour in air.

A sol-gel dip-coating process featuring aspects of slip casting was performed in a laminar flow (150 ft/min) chamber under clean room conditions (Class 100). To prepare a C6-surfactant templated silica (C6STS) sublayer, a membrane support tube was quickly dipped into the sol containing the C6-surfactant. After soaking for ten seconds, the membrane support was withdrawn at the rate of 7.6cm per minute. After drying, the

membrane was calcined at 120°C for one hour and was then confirmed to be impermeable to helium before surfactant removal by heating the membrane tube at 500°C for one hour in air. The same procedure was used to prepare membranes with other surfactant-templated silica sublayers. The as-prepared support tube with a C6STS layer was further dipped into the A2** sol using the above coating procedure. The as-coated membrane tube was heated under vacuum (<4 psia) at a heating rate of 1-2°C/min from room temperature to 300°C for six hours (membrane designated as AC300) or was then further calcined at 450°C in air for one hour (membrane designated as AC450).

Materials characterization

Corresponding bulk xerogels were characterized by thermal gravimetric analysis (TGA), differential thermal analysis (DTA) and nitrogen sorption porosimetry at 77 K (ASAP 2010, Micromeritics). Scanning electron microscopy (SEM,Hitachi S800) and transmission electron microscopy (TEM, Philips CM-30) were used to determine the morphology of membranes. Surface hydrophobicity of membranes was determined by water contact angle measurements (VCA-200 system). Thickness and refractive index of surfactant-templated and microporous films deposited on silicon wafers were measured using an ellipsometer (Gaertner® L116C). The film porosity was calculated using the Lorentz-Lorentz model, assuming a skeletal refractive index of 1.46 for silica [16].

A surface-acoustic-wave (SAW) unit integrated to a commercial porosimeter (ASAP 2010, Micromeritics) was used to determine pore accessibility of supported films

[17]. Adsorption of gas onto the surface of the SAW device causes a perturbation in the propagation velocity of the surface acoustic wave. The change of velocity could be further converted to the volume of gas adsorbed. The SAW-based sorption measurement with high sensitivity is advantageous in characterization of porous thin films prepared under membrane processing conditions.

Gas permeation

The gas permeation through the tubular silica membrane was measured using the apparatus depicted in Figure 1. Ambient moisture can easily condense inside silica micropores, it is thus extremely important to evacuate pores via an outgassing procedure prior to the startup of any permeation experiments [18]. The outgassing procedure is conducted at 80°C for at least three hours with dry helium purging across the membrane. The experimental procedure for determining gas permeance consisted of evacuating both sides of the membrane and then introducing pure gas or mixed gas into the tube side of the membrane. Single components such as He, H_2, CO_2, CO, N_2, NO and CH_4, and binary or multiple component mixtures were used for testing. The pressure at the tube side was maintained at a constant pressure (typically 6.5 bar). Meanwhile, the pressure at the shell-side gradually increased due to permeated gases. Upon exceeding atmospheric pressure, the shell side was opened to ambient pressure. To simulate practical operation, no sweeping gas was used and therefore the problem of a back diffusional flux could be eliminated. The flow rates of all inlet and outlet streams were directly measured by digital bubble flow meters (Humonics). In an extreme case where the permeate flow rate was

below the detectable limit of the digital bubble flow meter (~1 cc/min), the rate of pressure increase at the permeate side was converted to a permeate flow rate.

For mixed-gas permeation measurement, a pre-mixed gas with known composition was used and the compositions of both effluent streams were analyzed as functions of time using an on-line gas chromatograph. The flow rate and the pressure of the tube-side stream as well as the temperature of the membrane separator were varied. The experiments were continued until steady-state conditions (no change in flow rates and compositions with time) were reached. The change of gas-phase driving force (the partial-pressure gradient of component i, ΔP_i, across the membrane) along the membrane was taken into account; therefore, the permeance of the component i, $P_{m,i}$, was defined as

$$P_{m,i} = \frac{J_i}{\Delta P_{ln,i}}$$

$$where\ \Delta P_{ln,i} = \frac{(\Delta P_i)^I - (\Delta P_i)^{II}}{ln\{(\Delta P_i)^I / (\Delta P_i)^{II}\}}$$

where J_i was the steady-state flux of component i through the membrane. $(\Delta P_i)^I$ and $(\Delta P_i)^{II}$ were the partial-pressure differences of component i between the tube- and shell-side pressures of the membrane at the gas entrance (I) and exit (II) ends, respectively.

Separation factors defined by the ratio of permeabilities are equivalent to the ratio of permeances if membrane thickness is identical. Thus, for a single membrane tube, the ideal separation factor α_I for pure-gas permeation can be defined by the ratio of

permeances of individual pure gases. Analogous to the definition of α_I, the true separation factor α of mixed gas is defined by the ratio of permeances of constituent gases.

3. RESULTS AND DISCUSSION

The two most critical issues of processing sol-gel derived silica membranes are 1) avoiding defect formation, and 2) controlling pore sizes. Three strategies are employed to avoid or at least reduce defect formation. First, drying-induced stress as high as 200MPa in our silica sol system could result in film cracking unless the film thickness is below a critical cracking thickness h_c [19]. Through adjusting the sol concentration, withdrawal rate or sol aging time to maintain the membrane film thickness below the critical cracking thickness h_c (~4000Å for A2** sol), cracking is avoided. Second, membranes are processed under clean conditions to avoid foreign particles that could cause pinholes. Third, a surfactant-templated silica intermediate layer with pore size 10-20Å is used to 1) eliminate inherent defects on supports and 2) to facilitate the formation of subsequently deposited thin selective microporous membranes. The surfactant-templated silica sublayer is designed with both high porosity (~50 vol%) and low tortuosity to avoid creating additional flow resistance.

For pore size control, two strategies are 1) solvent (water)-templating [11], and 2) surfactant-templating [20]. Due to preferential alcohol evaporation during the film dip-coating process, water is the dominant solvent during the final stage of drying where the

pore size is established. Water molecules confined in the stressed film serve as templates to create pores of molecular dimension needed for molecular sieving. For the surfactant-templating strategy, surfactants (amphiphilic molecules composed of a hydrophilic head group and hydrophobic tail) are used as templates. Surfactant-templated silicas are high surface area amorphous solids (up to 1400 m^2/g) characterized by monosized pores, ranging normally from about 10-100Å in diameter, organized into periodic arrays that often mimic the liquid crystalline phases exhibited by surfactant-water systems. Both water and surfactants can be removed by heating to create pores with various dimensions. Combining the above strategies to process membranes with high selectivity and high flux is discussed further below.

Characterization of Surfactant-Templated Silica and Solvent-Templated Silica

Bulk xerogel was prepared by drying thin layers of silica sols on petri-dishes under ambient conditions. For as-prepared C6-surfactant templated silica (C6STS) bulk xerogel (Figure 2), differential thermal analysis (DTA) showed an endothermic peak near 200°C corresponding to the beginning of a drastic weight loss, indicating the decomposition of the C6-surfactant template. An exothermic peak at around 350°C was accompanied by a weight loss of about 45% attributed to the oxidative pyrolysis of surfactant and residual organics. N_2 sorption isotherms of the calcined C6STS thin film (calcined at 500°C for one hour), characterized by the SAW technique, appeared to be Type I, characteristic of microporous materials while that of a calcined C16-surfactant templated silica (C16STS) thin film appeared to be no hysteresis Type II, characteristic

of surfactant-templated mesoporous materials (Figure 3). Although N_2 sorption isotherms of calcined A2** *xerogel* appeared to be Type I with a very sharp increase of N_2 volume adsorbed within a relative pressure of 0 to 0.01 (Figure 3), indicating a small pore size and narrow pore size distribution, the corresponding thin film characterized using the SAW-based technique (data not shown) indicated no sorption of N_2 at 77K and Type-I sorption of CO_2 at dry ice temperature. These differences in pore size are attributed to differences in drying rates. Rapid drying of films avoids siloxane condensation, promoting the collapse of the silica network by the capillary stress. Based on a density functional theory (DFT) model, average pore diameters of the C6STS and C16STS were calculated at around 10-12Å and 18-20Å, respectively, with a narrow pore-size distribution, which is consistent with TEM observation. Furthermore, the surface area and porosity of the C6STS materials, calculated from N_2 sorption isotherms were 575 m^2/g and 28%, respectively. Porosity determined by ellipsometry agreed well with the result calculated from N_2 sorption isotherms. Detailed characterization of A2** and C16STS was reported by Sehgal and Brinker [11] and Lu et al. [20], respectively.

Membrane Configuration and Processing

The two-step coating procedure resulted in tubular membranes with gradual changes of pore size from 50Å (inner surface of commercial γ–alumina membrane) to 10-20Å (C6STS or C16STS sublayer), and then to 3-4Å (microporous A2** silica top-layer). Electron micrographs revealed the cross-section of an asymmetric supported

membrane (Figure 4a,b). The contrast difference between A2** (overlying microporous silica membrane) and the C6STS layer was due to differences in density. Due to lower porosity, the top A2** layer appears to be much denser than the C6STS sublayer composed of randomly oriented worm-like cylindrical pores. The plan-view of the A2** membrane layer (not shown) was featureless, suggesting a defect-free surface. The thickness of this A2** layer was around 30nm.

The dip-coating process, performed in a laminar flow (150ft/min) chamber under clean conditions (Class 100), and the sol pre-filtering step apparently prevented membranes from foreign-particle contamination during processing. Under clean conditions, membranes could be processed with better quality and reproducibility. One could imagine that 1μm foreign particles could easily penetrate through the thin top selective layer (~30nm), resulting in pinholes. As the top selective layer becomes thinner and thinner, such contamination control becomes ever more crucial.

The vacuum-calcination step affects the pore size and the stability of the pore structure. The A2** membrane layer was heated under vacuum (<4 psia) at a heating rate of 1-2°C/min from room temperature to 300°C for six hours to evacuate solvent and promote further pore shrinkage. The vacuum-calcination procedure also resulted in the decomposition of surface ethoxy groups, creating a surface deposit of amorphous carbon (visible as a black coating). Membrane surface caused an increase in the water contact angle from 17° to 41°, which may contribute to long-term membrane stability.

Gas Permeation

Silica has long been known to exhibit reversible CO_2 adsorption at room temperature [16]. Therefore, for the separation of CO_2 from other weakly adsorbable gases (e.g. O_2, N_2, CH_4) using silica membranes, one can expect an additional CO_2 surface flow at lower temperatures. In addition, preferential CO_2 adsorption inside micropores at low temperatures may enhance CO_2 selectivity due to the concomitant reduction of the pore aperture for weakly adsorbable gases. This phenomenon was also observed for a zeolitic membrane, where great differences between mixed-gas and single-gas permeation was measured due to preferential CO_2 adsorption [21]. In these cases, true gas separation strongly depends on feed composition and can not be directly represented by single-gas permeation under low-temperature operating conditions.

Comparison of membrane with or without sublayer

The surfactant-templated silica (STS) sublayers may serve to (1) eliminate intrinsic defects on porous supports and promote pore uniformity; therefore, increasing selectivity, and (2) prevent a subsequently deposited microporous overlayer from penetrating into support (the polysilicic clusters of the A2** sol are larger than the pore size of STS sublayers), thus enhancing flux. For membranes with only a C6STS or C16STS underlayer (without the microporous overlayer), gas transport occurred by Knudsen diffusion (probe gases, He and N_2). In contrast, for the dual-layer membrane, the microporous overlayer was capable of discriminating gas molecules such as He (2.6Å), H_2 (2.89Å), CO_2 (3.3Å), CH_4 (3.8Å), and N_2 (3.64Å) via molecular sieving (see further

discussion below). We also compared a single-layer microporous membrane (without STS sublayer) to the dual-layer membrane (AC300). At 60°C, the dual-layer membrane exhibited four-fold higher CO_2 permeances and four-fold higher CO_2/CH_4 selectivities than the single-layer membrane for pure gas permeation (Figure 5a,b). For the dual-layer membrane, ideal separation factors of various gas pairs (e.g. $\alpha_I(CO_2/CH_4) = 102$ at 25°C) largely exceeded Knudsen separation factors (e.g. $\alpha_K(CO_2/CH_4) = 0.6$).

For microporous gas diffusion, permeance is proportional to $\exp(-E_a/RT)$ under conditions maintaining a constant pressure gradient across the membrane, where E_a, R, and T are activation energy, gas constant and temperature, respectively [9]. In Figure 5a,b, for the dual-layer membrane, the exceptional negative activation energy of CO_2 (E_a = -3.37 KJ/mol) under a constant pressure gradient (ΔP=5.5bar) indicated the occurrence of CO_2 capillary condensation, where CO_2 transported with high density through narrow pores at lower temperatures. On the contrary, CO_2 capillary condensation was less significant for the single-layer membrane; therefore, a gradual increase in CO_2 permeance with temperature (activated transport) was observed (E_a=2.48 KJ/mol). Moreover, the activation energy of CO_2 was much lower than that of CH_4. The activation energy of CH_4 transport was 9.64 KJ/mol for the single-layer membrane and 12.92 KJ/mol for the dual-layer membrane. This showed that CH_4 diffused through the membrane mainly via activated transport. This also suggested that, compared to single-layer membranes, dual-layer membranes exhibit a much narrower pore-size distribution. The combination of the CO_2 condensation effect and CH_4 activated transport can well explain the drastic increase

in ideal separation factor of CO_2/CH_4 upon decrease in temperature, particularly, for the dual-layer membrane (Figure 5b).

This sublayer effect was demonstrated again in other surfactant-templating systems. Mesoporous C16STS materials showed the same sublayer effect as the microporous C6STS materials. A new approach was developed to prepare a continuous mesophase surfactant-templated silica sublayer for improvement of a subsequently deposited microporous membrane. A commercial 50Å γ-Al_2O_3 membrane tube was dip-coated into the C16STS sol followed by calcination to remove the surfactant template. The membrane was further dipped into a (bis(triethoxysilyl)ethane) (BTE) silica sol, prepared by mixing BTE into TEOS (tetraethoxysilane) together with ethanol, H_2O and HCl in a molar ratio of 0.8: 0.2: 3.8: 5.1: 5.3×10^{-3}. The ethane ligands ($-CH_2CH_2-$) of the BTE embedded in the silica framework were removed by calcination at 280°C for three hours, creating micropores. A comparison of the membranes with and without a mesoporous sublayer is shown in Figure 6a,b. Results again suggested that dual-layer membranes with a mesoporous sublayer exhibit higher permeance and better selectivity than the single-layer membrane without a sublayer. This consistent behavior implied the crucial role of the sublayer in improving both flux and selectivity of an overlying microporous silica membrane. Furthermore, the same concept can be extended to the use of an *ordered* mesoporous silica membrane as a sublayer to minimize transport resistance. For example, a nonionic block copolymer surfactant ($CH_3(CH_2)_{15}(CH_2CH_2O)_{10}OH$, Brij56), was used as a structure-directing agent in place of ionic surfactants (e.g. C6- and

C16-surfactant). The Brij56 surfactant-templated silica with both high porosity (64%) and an *ordered* cubic structure (uniform pore size ~23Å) is a promising candidate for use as a sublayer for a subsequently deposited microporous membrane (Figure 7).

Permeance and CO_2/CH_4 separation factor as function of feed flow rate, temperature and pressure gradient

The effect of temperature, flow rate, and pressure gradient across the dual-layer membrane (AC300) on both CO_2 permeance and CO_2/CH_4 separation factor was investigated via mixed-gas (50/50 (v/v) CO_2/CH_4) permeation experiments under steady-state conditions. For the investigation of the feed flow-rate effect, experiments were performed at constant temperature (26°C) while maintaining a constant pressure gradient across the membrane (ΔP=5.5bar) (Figure 8a,b). The stage cut, θ, defined as the ratio of permeate to feed flow rate, represents the fraction of feed gas permeated through the membrane. θ is increased by decreasing the feed flow rate but at the expense of the purity of CO_2 recovered at permeate side (Figure 8a). At a high feed flow rate (low stage cut), the concentration of the fast permeating gas, CO_2, remained high at the retentate side; therefore, a high CO_2 driving force across the membrane was maintained. This allowed CO_2 molecules to pass through the membrane pores with maximal driving force and less hindrance by larger CH_4 molecules (Figure 8b). This also indicated that flux and separation factor were strong function of retentate compositions in the mixed-gas mode.

The CO_2 permeance and $\alpha(CO_2/CH_4)$ can reach as high as 3×10^{-4} $cm^3(STP)/(s\cdot cm^2\cdot cm\text{-}Hg)$ and over 200, respectively, by increasing the feed flow rate.

For the investigation of the effect of temperature, experiments were conducted at a constant feed flow rate while maintaining a constant pressure gradient across the membrane. The steady-state values of CO_2 permeance and separation factor, $\alpha(CO_2/CH_4)$, were assured by reversible heating and cooling. Figure 9 shows that CO_2 permeance increases slightly with temperature while the $\alpha(CO_2/CH_4)$ decreases with temperature. The slight increase in CO_2 permeance with temperature suggested that in the presence of CH_4, CO_2 transport is slightly activated by temperature. The drastic increase in $\alpha(CO_2/CH_4)$ at lower temperature was similar to what was observed for pure-gas permeation (Figure 5a). Moreover, at lower temperature, the mixed-gas $\alpha(CO_2/CH_4)$ at high feed flow rate was always higher than the pure-gas $\alpha_I(CO_2/CH_4)$. This is due to preferential adsorption of CO_2 inside the pores, under which mixed-gas feed conditions, thus hinders the CH_4 transport through the membranes. Comparing Figure 5a to Figure 9, the difference between $\alpha(CO_2/CH_4)$ and $\alpha_I(CO_2/CH_4)$ vanishes at higher temperatures owing to the decrease in CO_2 adsorption.

For investigation of the effect of pressure, the retentate pressure was varied while the permeate pressure was maintained at ambient atmospheric pressure (Figure 10). Figure 10 shows that, under constant feed flow rate and temperature conditions, the $\alpha(CO_2/CH_4)$ is essentially independent of the pressure gradient while the CO_2 permeance slightly increases with pressure gradient and then levels off at higher pressure gradients.

The initial increase in CO_2 permeance might be indicative of low CO_2 coverage on pore walls at a low pressure gradient. At higher pressure, once the pore walls were covered with CO_2, transport was independent of the pressure gradient.

The dual-layer membrane was operated for 150 hours under constant temperature, pressure gradient, and feed flow rate conditions (Figure 11). Due to the gradual removal of pre-adsorbed moisture during this extended permeation test, both the CO_2 permeance and $\alpha(CO_2/CH_4)$ gradually increased with time. Nevertheless, stable and continuous operation could be achieved at room temperature. A mathematical model for a multilayer membrane module, accounting for the influence of a number of operating parameters (temperature, pressure, and feed flow rates) will be presented elsewhere [22].

Processing membranes under higher calcination temperature for hydrogen purification and NO_x removal

The dual-layer membrane processed at 300°C (AC300) was excellent for CO_2/CH_4 separation but was unable to achieve outstanding H_2 separation due to its relatively large pore size. Pore size could be further reduced via an extended calcination step at 450°C for one hour in air (membrane designated as AC450). Pure-gas permeation for the AC450 membrane at 80°C is shown in Figure 12. Due to the extended calcination, the pore size of the membrane was further reduced, resulting in a sharp molecular-size cut-off near 3.5Å. With an excellent hydrogen separation factor (H_2/CH_4 = 1265) as well as a high hydrogen permeance (1×10^{-3} cm^3(STP)/cm^2/s/cmHg), such a membrane provides a great

opportunity in applications such as hydrogen recovery from petrochemical plants and hydrogen purification for fuel cells. Of relevance to fuel cells, the membrane selectively separated hydrogen from a simulated reformate gas mixture that would result from the partial oxidation of methanol (33.98% N_2, 15.00% CO_2, 0.997% CO, balance H_2). A 92 mole% H_2 purity could be obtained in the permeate stream at a stage-cut of 8.2% (see Table 1). The CO concentration (CO is a known PEM fuel cell poison) in the permeate stream was reduced to at least fifty times lower than that in the feed. We also achieved a high H_2 permeance (6 x 10^{-4} cm^3(STP)/s/cm^2/cmHg) and a high H_2/N_2 separation factor of over 270 for separation of a 50/50 (v/v) H_2/N_2 gas mixture (Table 2). Beside H_2 purification, the membrane could also be used in NO_x removal from power-plant flue gas. NO/N_2 selectivity and NO permeance reached 9.3 and 3×10^{-5} cm^3(STP)/cm^2/s/cmHg, respectively, for pure-gas permeation (Figure 13).

Comparison

By operating at room temperature, a moderate pressure gradient (ΔP=5.5 bar), and a high feed flow rate (~500 cm^3 (STP)/min), we achieved a high CO_2 permeance (3.2 x 10^{-4} cm^3(STP)/s/cm^2/cmHg) and a high CO_2/CH_4 separation factor of over 200 for separation of a 50/50 (v/v) CO_2/CH_4 gas mixture. The AC300 membrane with a combination of high permeance and high selectivity was superior to reported gas separation membranes, while the AC450 membrane has a higher CO_2/CH_4 separation factor (~600) at the expense of CO_2 permeance (Figure 13). It is difficult to compare various types of membranes under

the same membrane operation conditions since reported membranes made of different materials were all operated under different conditions to achieve their best performance. For example, polyimide membranes tend to be operated with a low CO_2-partial-pressure feed stream to alleviate CO_2 plasticization [23]. Polyelectrolyte membranes based on facilitated transport were also operated with low CO_2-partial-pressure feed streams to achieve higher CO_2 permeance [24]. Some silica membranes were operated at higher temperatures with sweeping gas [9] while zeolite Y membranes were operated at room temperature to benefit from CO_2 selective adsorption [21]. However, our dual-layer membranes still show superior performance when compared to reported membranes operated at their optimum conditions.

4. CONCLUSIONS

The quality of the support is crucial for the quality of overlying membrane layer. Pinholes and surface roughness on the support normally produce defects in the subsequently deposited membrane. Thus, we designed a new protocol to ameliorate membrane performance and reproducibility by improving support surface and processing conditions. First, we deposited a surfactant-templated micro- or mesoporous intermediate layer on top of a commercial γ–alumina support to both improve surface finish and prevent the subsequently deposited sol from penetrating into the support. Second, membranes were dip-coated under class 100 clean room conditions to avoid dust contamination and were vacuum-calcined at 300°C for six hours to promote further pore

shrinkage. The vacuum calcination procedure apparently also resulted in the decomposition of surface ethoxy groups; therefore, a more hydrophobic pore surface was formed as evidenced by an increase in the water contact angle. The dual layer approach enhanced both flux and selectivity of an asymmetric membrane with gradual changes of pore size from 50Å (γ–alumina support layer) to 10-12Å (surfactant-templated silica intermediate layer), and then to 3-4Å (30nm thick, microporous silica top-layer). The novel membrane synthesis and processing technique could be potentially adapted to processing a thin, highly selective sol-gel coating on a high-surface-area polymeric hollow fiber (or ceramic monolith) support.

With the combination of high flux and high selectivity (CO_2 permeance of $(3\sim0.5)\times10^{-4}$ $cm^3(STP)/(s\cdot cm^2\cdot cm\text{-}Hg)$ and CO_2/CH_4 separation factor of 200~600), the dual-layer silica membrane was superior to all other reported membranes for separation of a 50/50 (v/v) CO_2/CH_4 gas mixture. Upon further calcination, the efficiency of separating H_2 from constituent gases was enhanced due to shrinkage of larger pores. The membrane selectively separated hydrogen from a simulated reformate mixture (33.98% N_2, 15.00% CO_2, 0.997% CO, Balance H_2) for application in fuel cells as evidenced by the high concentration of hydrogen recovered in the permeate side stream. A 92 mole% H_2 purity could be obtained in the permeate stream. The CO concentration (CO is a fuel cell poison) in the permeate was reduced to at least fifty times lower than that in the feed. Beside H_2 purification, the membrane can also be applied to NO_x removal from flue gas. NO/N_2 selectivity and NO permeance reached 9.3 and 3×10^{-5} $cm^3(STP)/cm^2/s/cmHg$,

respectively. The combined strategies are proved to be effective for achieving molecular sieving in inorganic silica membranes. The subject dual-layer silica membrane could find great use in applications such as purification of sub-quality natural gas, removal of NO_x from power-plant flue gas, reduction of green house gases (e.g. CO_2) and hydrogen recovery from processing gases or hydrogen purification for fuel-cell applications.

ACKNOWLEDGEMENTS

The authors are very grateful for the financial support from the Electric Power Research Institute, the U.S. Department of Energy Federal Energy Technology Center and the Sandia National Laboratory, Laboratory Directed Research and Development Program. H. Fan, S. Naik and Dr. T.J. Gardner are acknowledged for fruitful discussions and technical assistance. This work was performed at Sandia National Laboratories and supported by the U.S. Department of Energy under Contract No. DE-AC04-94AL85000

REFERENCES

1. R.W. Spillman, Economics of Gas Separation Membranes, *Chem. Eng. Prog.*, **85**(1) (1989) 41-62

2. R.W. Baker, E.L. Cussler, W. Eykamp, W.J. Koros, R.L. Riley, H. Strathmann, Membrane Separation Systems - A Research & Development Needs Assessment, *US DOE Report, DE-AC01-88ER30133* (1990).

3. J.N. Armor, Membrane Catalysis: Where Is It Now, What Needs To Be Done, *Catal. Today*, **25**(3-4) (1995) 199-207.

4. C.-Y. Tsai, A.G. Dixon, Y.H. Ma, W.R. Moser, and M.R. Pascucci, Dense Perovskite $La_{1-x}A'_xFe_{1-y}Co_yO_{3-\delta}$ (A' = Ba, Sr, Ca), Membrane Synthesis, Applications, and Characterization, *J. Am. Ceram. Soc.*, **81**(6) (1998) 1437-1444.

5. C.J. Brinker, T. L. Ward, R. Sehgal, N. K. Raman, S. L. Hietala, D. M. Smith, D. W. Hua and T. J. Headley, 'Ultramicroporous' Silica-Based Supported Inorganic Membranes, *J. Membr. Sci.*, **77** (1993) 165-179.

6. C.J. Brinker, R. Sehgal, S.L. Hietala, R. Deshpande, D.M. Smith, D.Loy and C.S. Ashley, Sol-gel Strategies for Controlled Porosity Inorganic Materials, *J. Membr. Sci.*, **94** (1994) 85.

7. N.K. Raman and C. J. Brinker, Organic "Template" Approach to Molecular Sieving Silica Membranes, *J. Membr. Sci.*, **105** (1995) 273-279.

8. R.S.A. De Lange, J.H.A. Hekkink, K. Keizer and A.J. Burggraaf, Formation and Characterization of Supported Microporous Ceramic Membranes Prepared by Sol-Gel Modification Techniques, *J. Membr. Sci.*, **99** (1995) 57-75.

9. R.M. De Vos and H. Verweij, Improved Performance of Silica Membranes for Gas Separation, *J. Membr. Sci.,* **143**(1-2) (1998) 37-51.

10. L.C. Klein and D. Gallagher, Pore Structure of Sol-Gel Silica Membrane, *J. Membr. Sci.*, **39**(3) (1988) 213-220

11. R. Sehgal and C.J Brinker, Supported Inorganic Membrane, *US patent 5,772,735* (1998).

12. R.P. Beaver, Method of Producing Porous Hollow Silica-Rich Fibers, *US Patent 4,778,499* (1998).

13. G.R. Gavalas, C.E. Megiris C.E. and S.W. Nam, Deposition of H_2 Permselective SiO_2-films, *Chem. Eng. Sci.* , **44**(9) (1989) 1829-1835.

14. A.J. Burggraaf and L. Cot, Fundamentals of Inorganic Membrane Science and Technology, Ed. A.J. Burggraaf and L. Cot, Elsevier, Amsterdam (1996) 1-20

15. C.J. Brinker, K.D. Keefer, D.W. Schaefer, and C.S. Ashley, Sol-Gel Transition in Simple Silicates, *J. Non-Crystalline Solids*, **48** (1982) 47-64.

16. C.J. Brinker and G.W. Scherer, Sol-Gel Science, Academic Press (1990) 803.

17. S.L. Hietala, D.M. Smith, V.M. Hietala, G.C. Frye and S.J. Martin, Pore Structure Characterization of Thin Films Using a Surface Acoustic Wave/ Volumetric Adsorption Technique, *Langmuir*, **9** (1993) 249-251.

18. C.-Y. Tsai and C.J. Brinker, Silica Gas Separation Membranes Prepared with Surfactant-Templated Sublayers, *Proc. Fifth Int. Conf. on Inorg. Memb.*, Ed. S.-I. Nakao (1998) 180-183.

19. M.D. Thouless, Decohesion of Films with Axisymmetric Geometries, Acta Metall. **36**(12) (1988) 3131-3135.

20. Y.F. Lu, R. Ganguli, C.A. Drewien, M.T. Anderson, C.J. Brinker, W.L. Gong, Y.X. Guo, H. Soyez, B. Dunn, M.H. Huang and J.I. Zink, Continuous Formation of Supported Cubic and Hexagonal Mesoporous Films by Sol-Gel Dip-Coating, *Nature*, **389** (1997) 364-368.

21. K. Kusakabe, T. Kuroda, A. Murata and S. Morooka, Formation of a Y-Type Zeolite Membrane on a Porous Alpha-Alumina Tube for Gas Separation, *Ind. Eng. Chem. Res*, **36**(3) (1997) 649-655.

22. S.-Y. Tam, C.-Y. Tsai and C.J. Brinker, Mathematical Modeling of Microporous Silica Membrane Module for CO_2 Removal from Natural Gas, to be published.

23. L.S. White, T.A. Blinka, H.A. Kloczewski and I.F. Wang, Properties of a Polyimide Gas Separation Membrane in Natural-Gas Streams, *J. Memb. Sci.*, **103**(1-2) (1995) 73-82.

24. R. Quinn, A Repair Technique for Acid Gas Selective Polyelectrolyte Membranes, *J. Memb. Sci.*, **139**(1) (1998) 97-102.

List of Tables

List of Figures

silica film templated by Brij56 block-copolymer surfactant ($CH_3(CH_2)_{15}(CH_2CH_2O)_{10}OH$), and (c) microporous layer.

Figure 8a,b. CO_2 permeance and CO_2/CH_4 separation factor α as a function of feed flow rate for separation of a 50/50 (v/v) CO_2/CH_4 gas mixture, (a) $\%CO_2$ in permeate and CO_2/CH_4 separation factor vs. stage cut (stage cut = ratio of permeate to feed flow rate), (b) CO_2 permeance and CO_2/CH_4 separation factor vs. feed flow rate

Figure 9. CO_2 permeance and CO_2/CH_4 separation factor α as a function of temperature for separation of a 50/50 (v/v) CO_2/CH_4 gas mixture.

Figure 10. CO_2 permeance and CO_2/CH_4 separation factor α as a function of pressure gradient for separation of a 50/50 (v/v) CO_2/CH_4 gas mixture.

Figure 11. AC300 membrane separator continuously operated for 150 hours under conditions of constant temperature, pressure gradient, and feed flow rate

Figure 12. Molecular-sieving behavior of an AC450 membrane. The ideal separation factor α_I, represents the ratio of permeance (measured in pure-gas permeation tests) for two specified gases.

Figure 13. Comparison of reported membranes for a mixed-gas, CO_2/CH_4 separation, (a) present A2**/C6 membrane, AC300 and AC450, (b) silica membrane from ref. [9] (CO_2 permeance at 100°C estimated from reported single-component permeation) (c) polyelectrolyte (PVBTA) membrane[24], (d) polyimide membrane[23], and (e) zeolite membrane[21]

Table 1.

Gas i	Permeance $\times 10^6$ (cm^3(STP)/s/cm^2/cmHg)	Separation Factor (H_2/Gas i)	Pure-gas permeance ratio	Permeate (mole%)	Retentate (mole%)
H_2	507	-	-	92.19	43.25
CO_2	101	5.0	5.2	7.36	16.89
N_2	2.15	235.9	316.0	0.37	40.47
CO	3.83	132.2	198.6	0.0193	1.14

tube-side pressure = 6.5 bar; stage cut = 8.2%

Table 2.

Gas i	Permeance $\times 10^6$ (cm^3(STP)/s/cm^2/cmHg)	Separation Factor (H_2/Gas i)	Pure-gas permeance ratio	Permeate (mole%)	Retentate (mole%)
H_2	606	-	-	99.41	37.43
N_2	2.21	274.5	316.0	0.59	62.57

tube-side pressure = 6.5 bar; Stage cut = 11%

Figure 1.

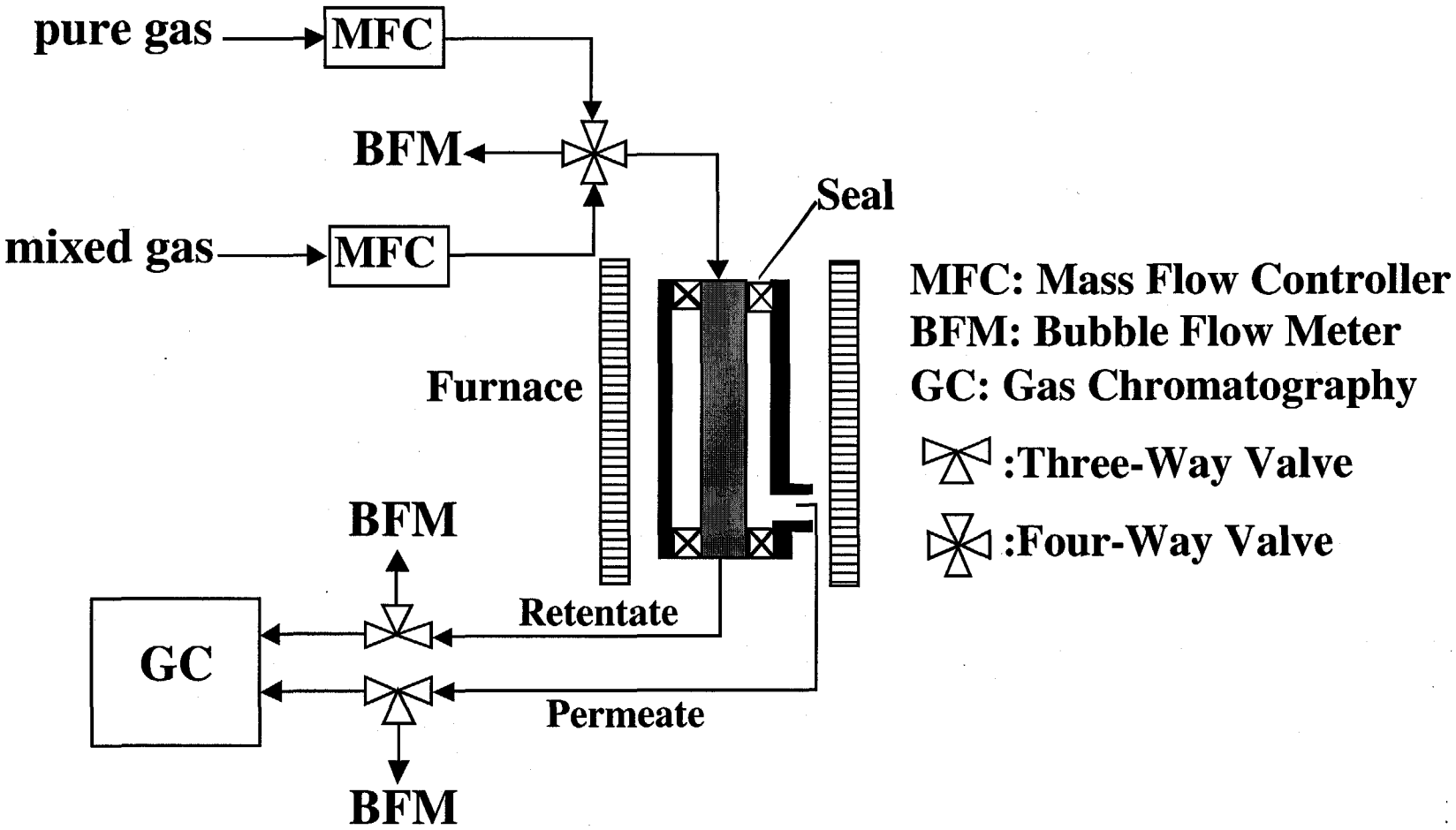
pure gas
MFC
BFM
mixed gas
MFC
Seal
Furnace
BFM
GC
Retentate
Permeate
BFM
MFC: Mass Flow Controller
BFM: Bubble Flow Meter
GC: Gas Chromatography
:Three-Way Valve
:Four-Way Valve

Figure 2.

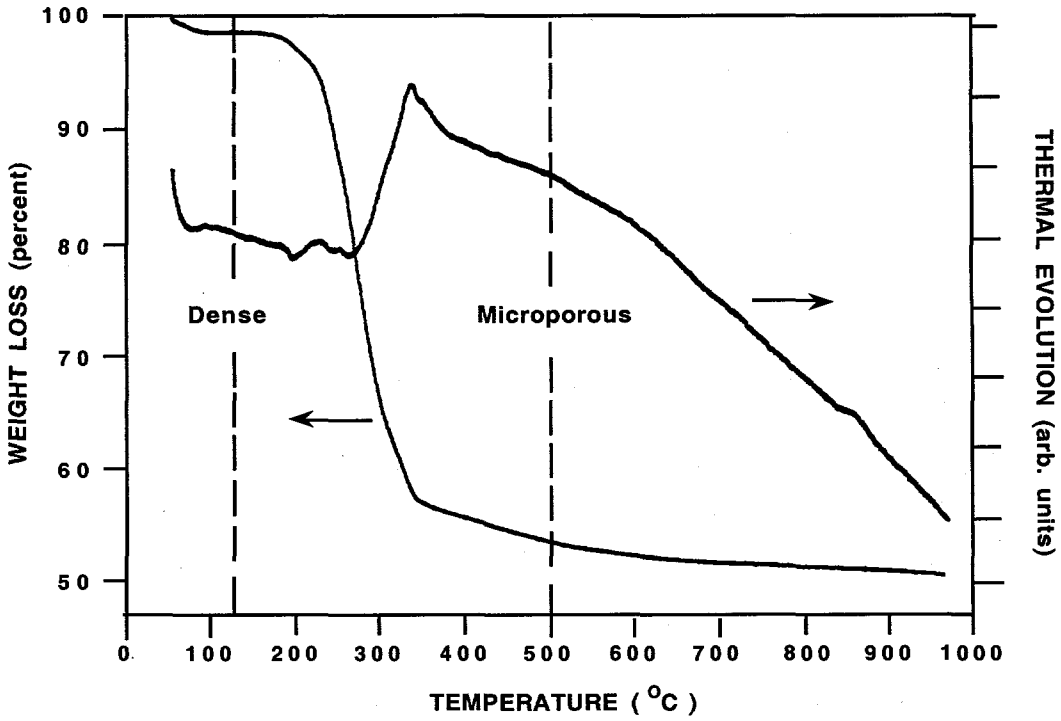
100
90
80
70
60
50
WEIGHT LOSS (percent)
THERMAL EVOLUTION (arb. units)
Dense
Microporous
0
100
200
300
400
500
600
700
800
900
1000
TEMPERATURE (°C)

Figure 3.

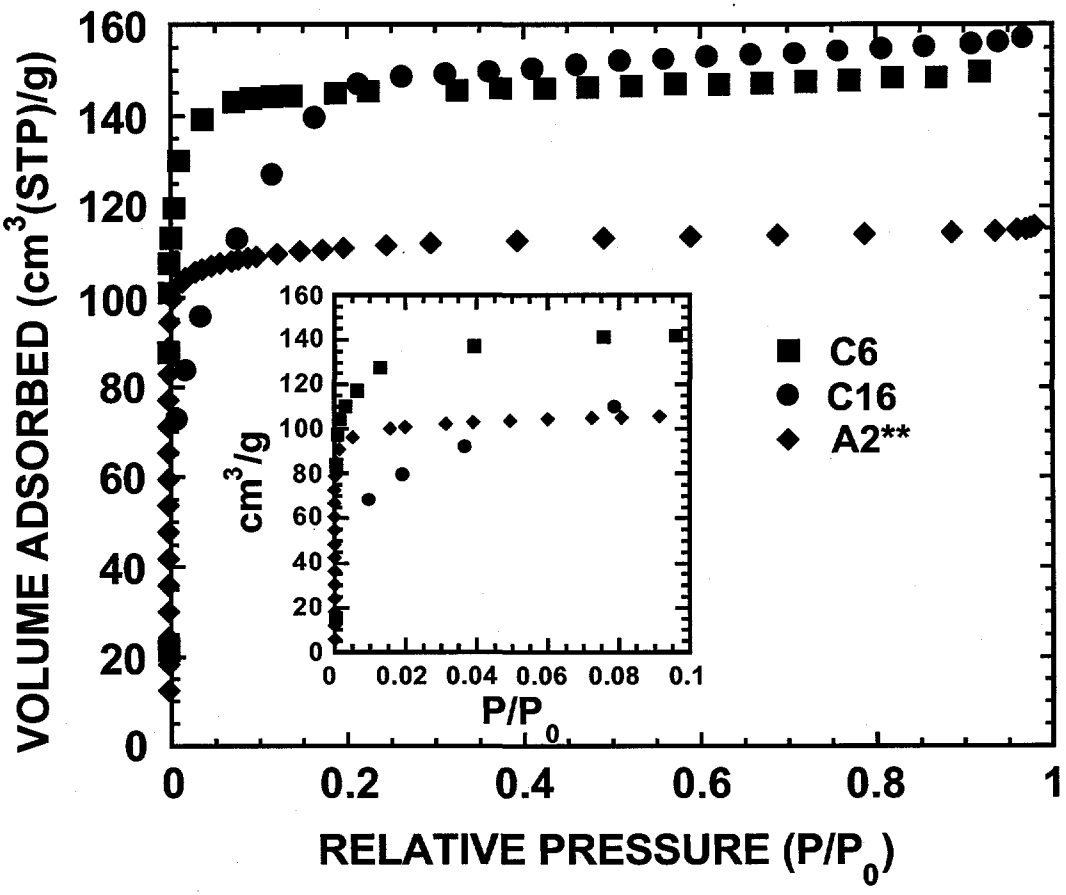
VOLUME ADSORBED (cm^3(STP)/g)
RELATIVE PRESSURE (P/P$_0$)
C6
C16
A2**
cm^3/g
P/P$_0$

Figure 4a,b

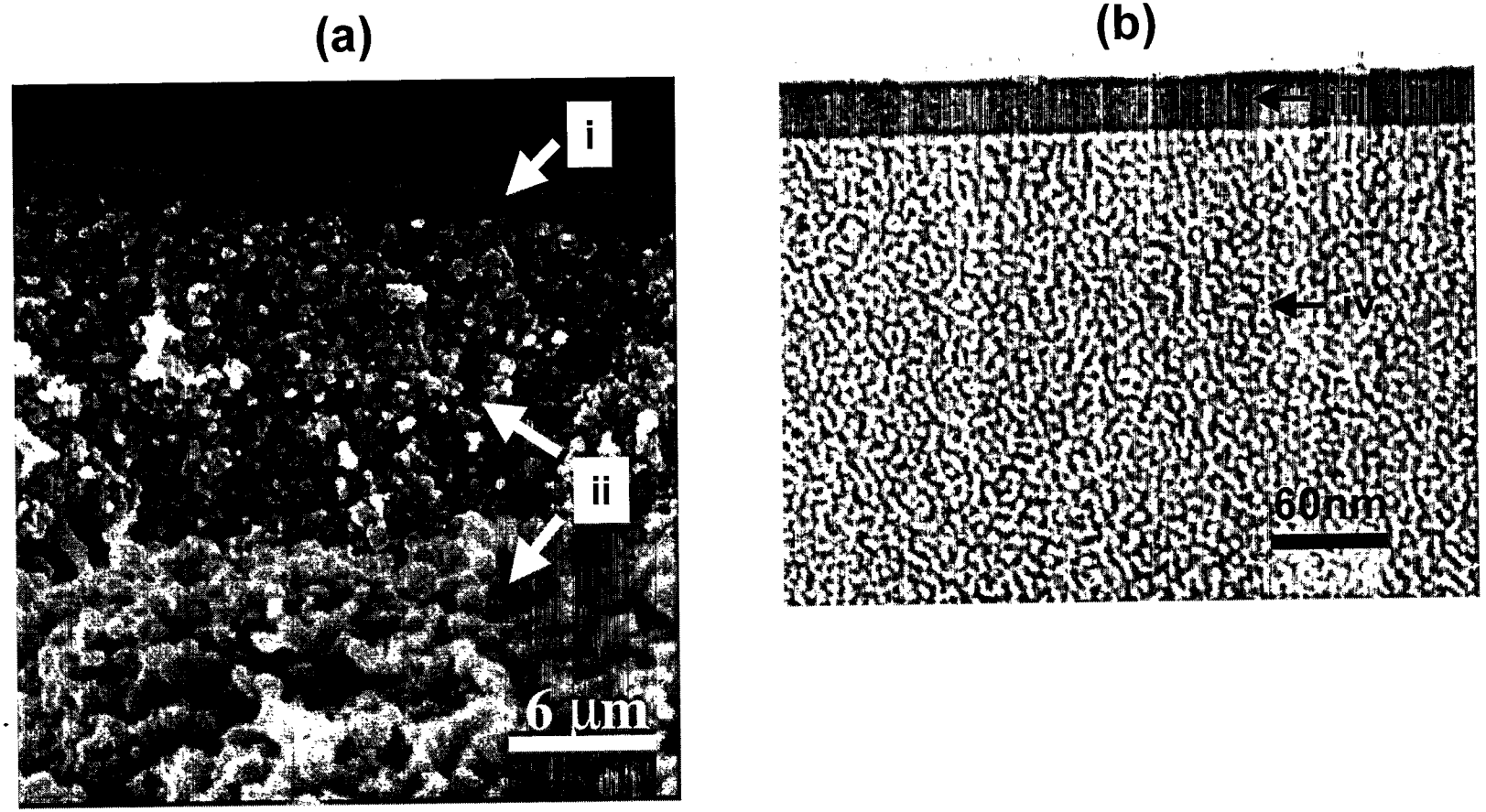

Figure 5a,b.

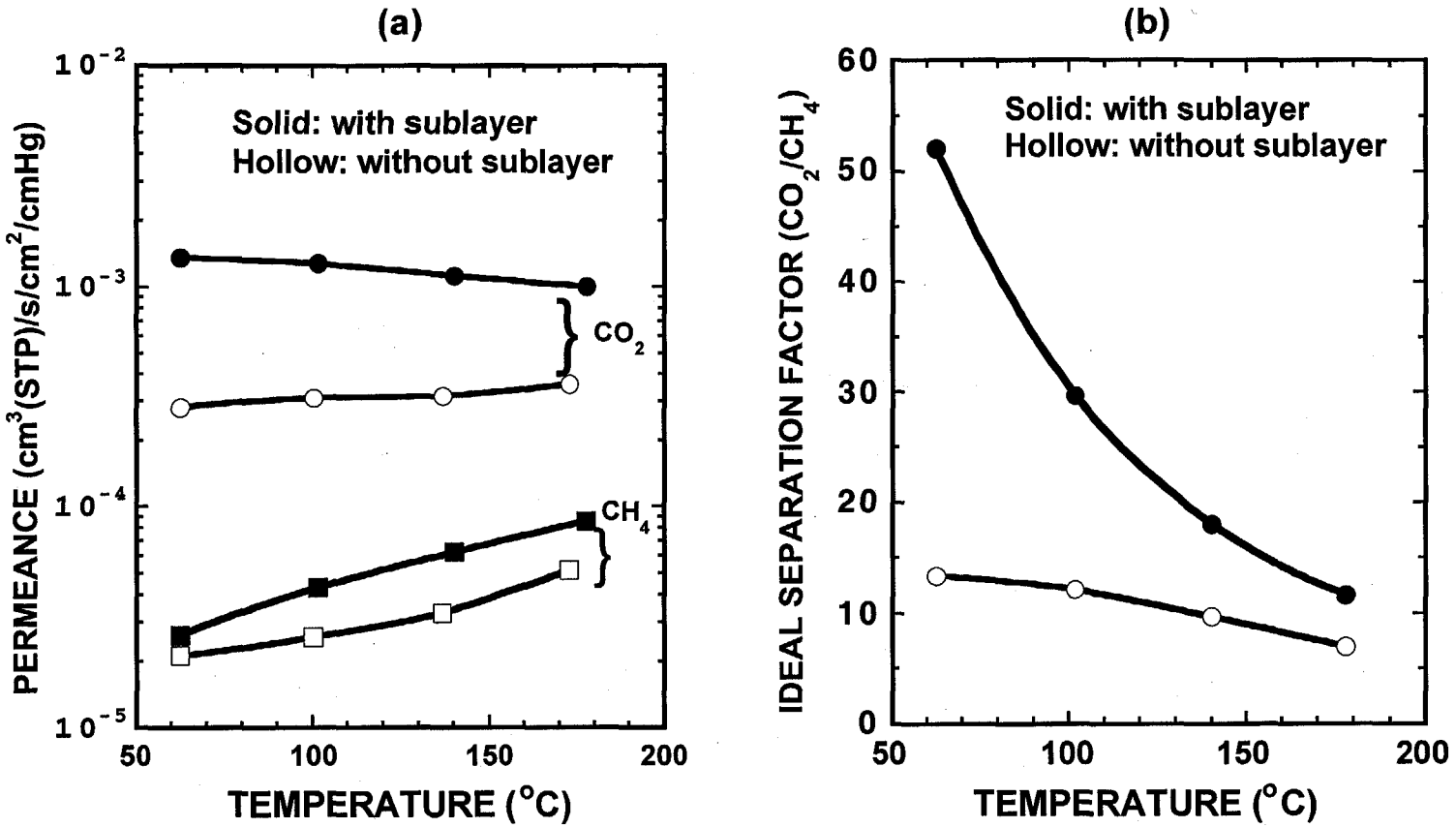
(a)
Solid: with sublayer
Hollow: without sublayer
CO2
CH4
PERMEANCE (cm3(STP)/s/cm2/cmHg)
10-2
10-3
10-4
10-5
50
100
150
200
TEMPERATURE (°C)
(b)
Solid: with sublayer
Hollow: without sublayer
IDEAL SEPARATION FACTOR (CO2/CH4)
60
50
40
30
20
10
0
50
100
150
200
TEMPERATURE (°C)

Figure 6a,b.

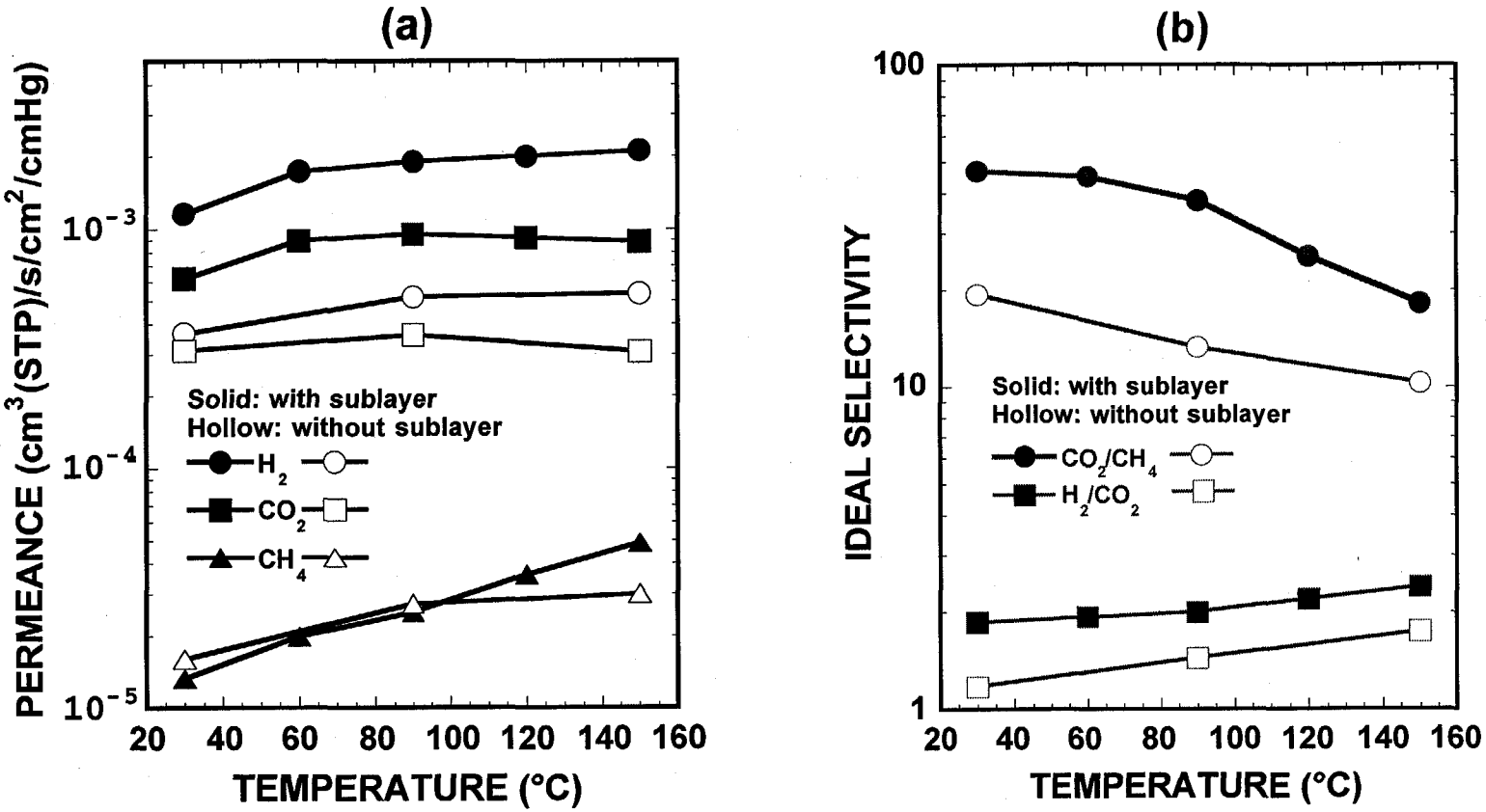
(a)
PERMEANCE (cm3(STP)/s/cm2/cmHg)
10-3
10-4
10-5
Solid: with sublayer
Hollow: without sublayer
H2
CO2
CH4
20 40 60 80 100 120 140 160
TEMPERATURE (°C)
(b)
IDEAL SELECTIVITY
100
10
1
Solid: with sublayer
Hollow: without sublayer
CO2/CH4
H2/CO2
20 40 60 80 100 120 140 160
TEMPERATURE (°C)

Figure 7.

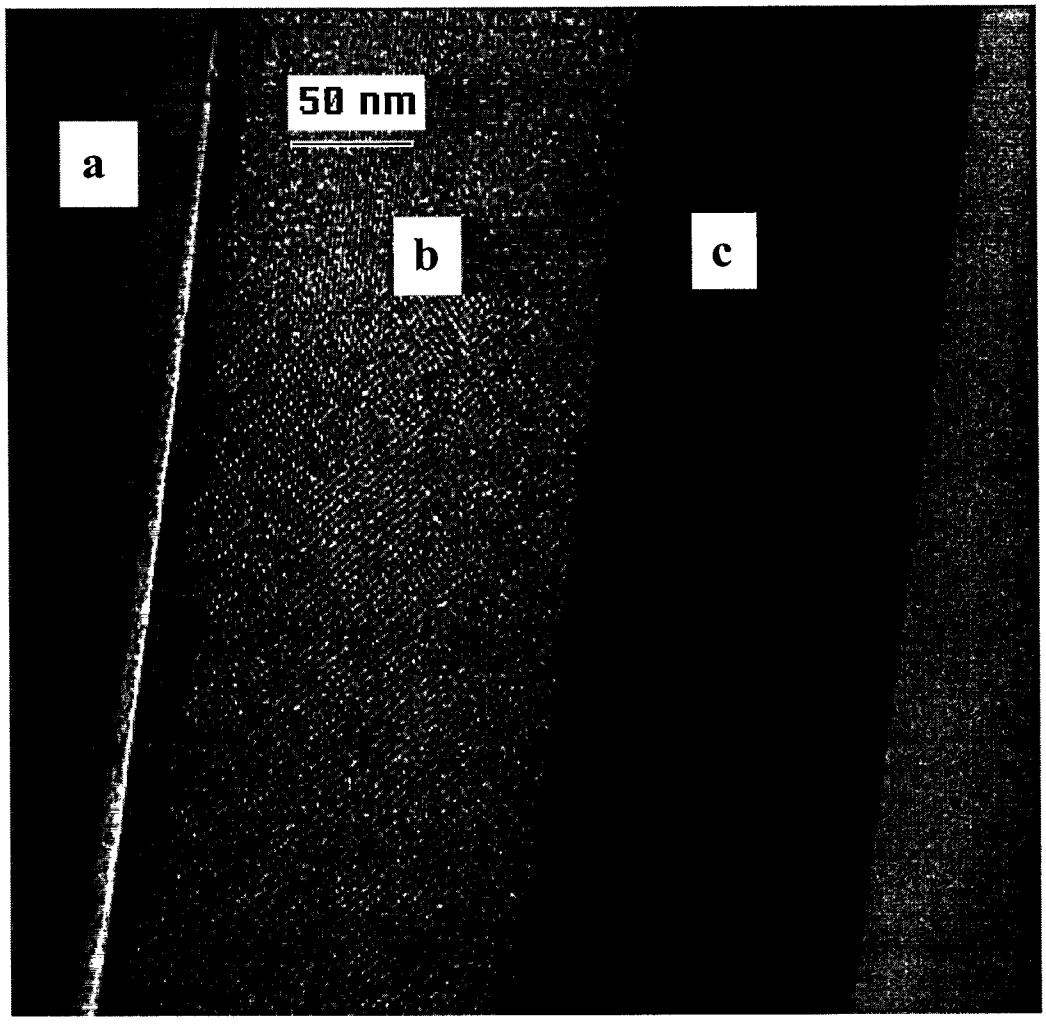

Figure 8a,b

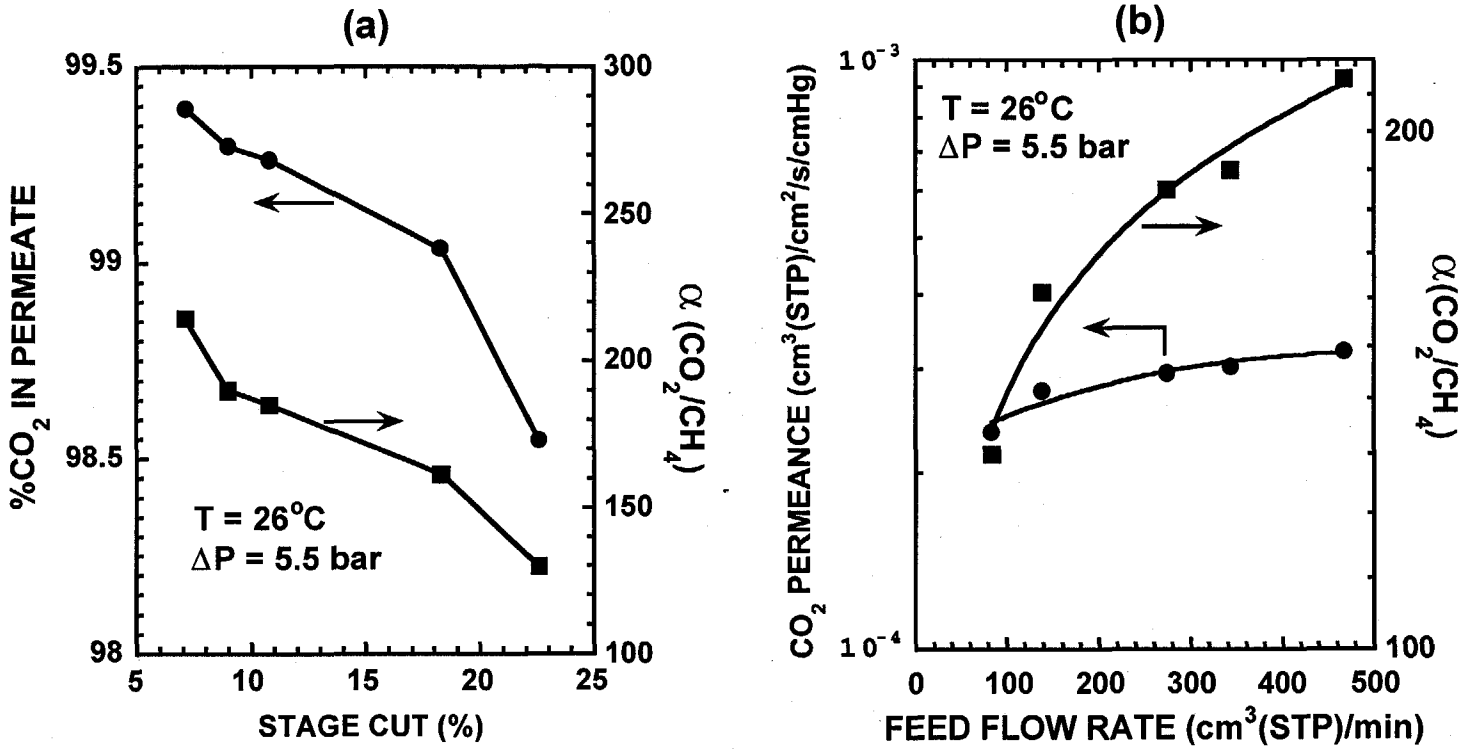
(a)
99.5
99
98.5
98
300
250
200
150
100
5
10
15
20
25
%CO2 IN PERMEATE
α (CO2/CH4)
STAGE CUT (%)
T = 26°C
ΔP = 5.5 bar
(b)
10-3
10-4
200
100
0
100
200
300
400
500
CO2 PERMEANCE (cm3(STP)/cm2/s/cmHg)
α(CO2/CH4)
FEED FLOW RATE (cm3(STP)/min)
T = 26°C
ΔP = 5.5 bar

Figure 9

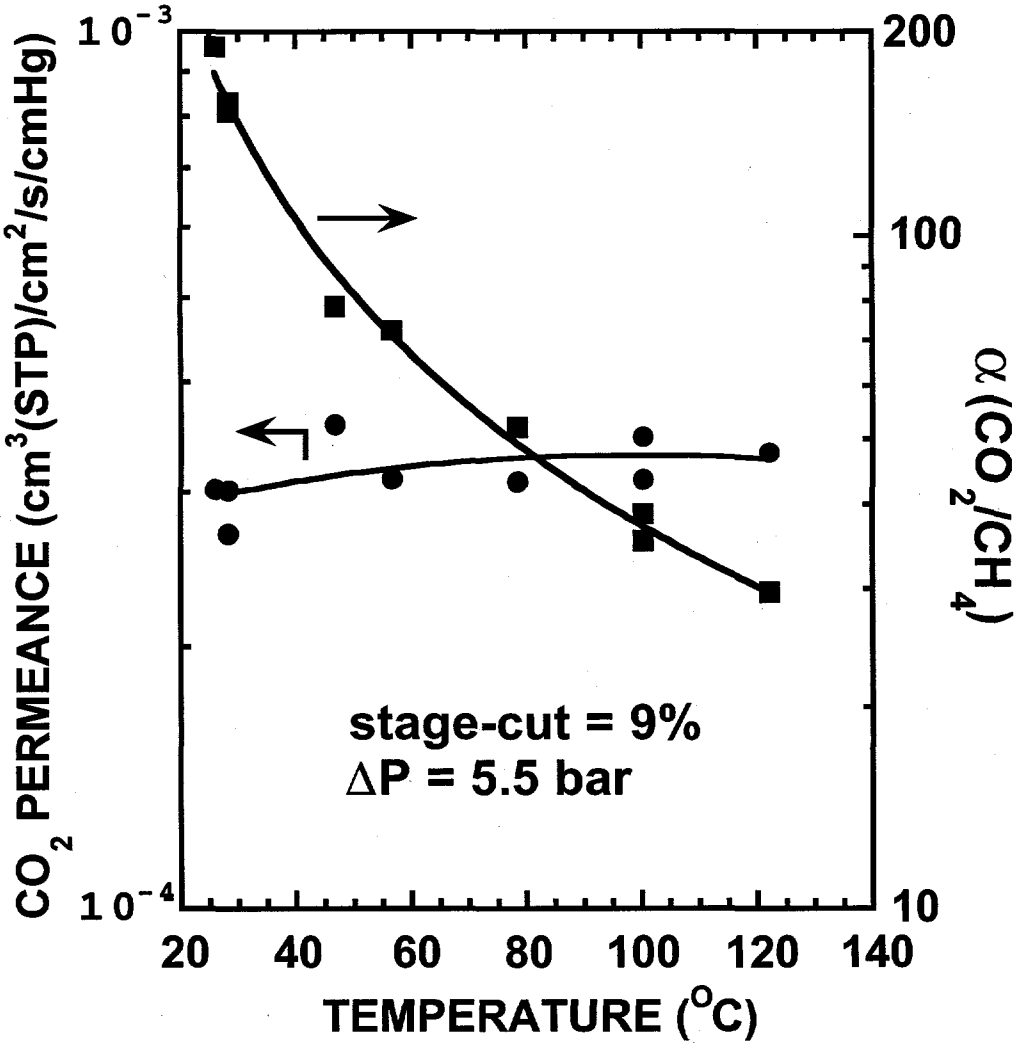
10^{-3}
10^{-4}
CO_2 PERMEANCE (cm^3(STP)/cm^2/s/cmHg)
200
100
10
α (CO_2/CH_4)
stage-cut = 9%
ΔP = 5.5 bar
20
40
60
80
100
120
140
TEMPERATURE (^{O}C)

Figure 10

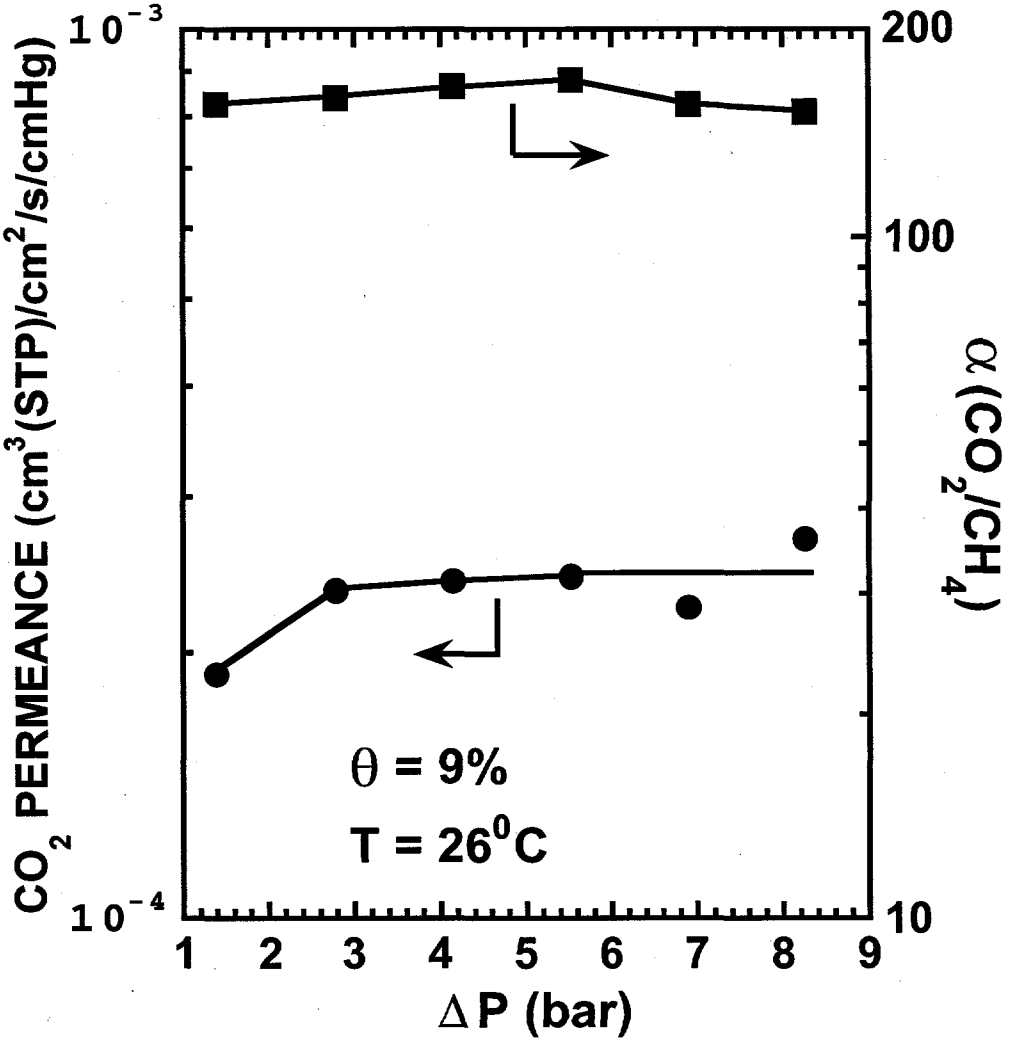
10^{-3}
10^{-4}
CO_2 PERMEANCE (cm^3(STP)/cm^2/s/cmHg)
200
100
10
α (CO_2/CH_4)
θ = 9%
T = 26^0C
1 2 3 4 5 6 7 8 9
ΔP (bar)

Figure 11

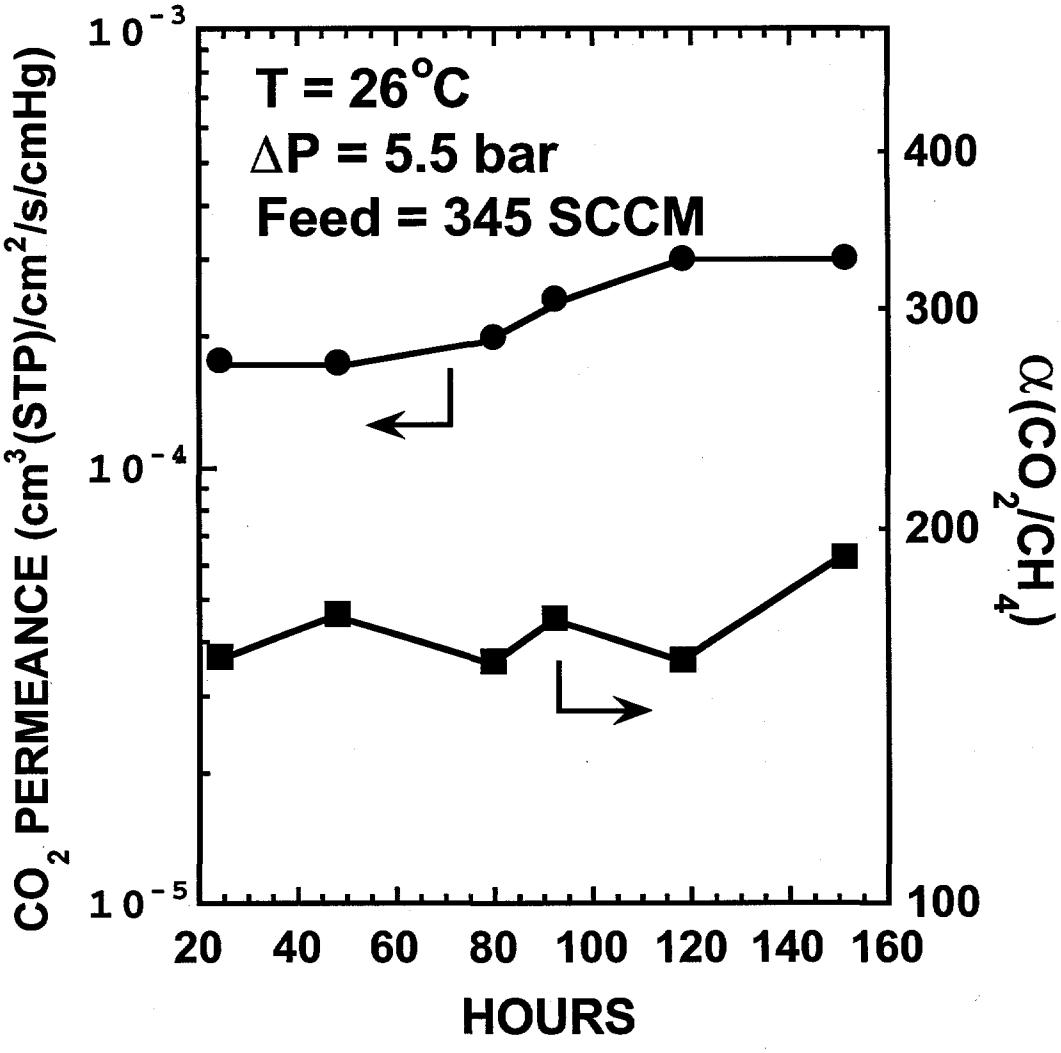
T = 26°C
ΔP = 5.5 bar
Feed = 345 SCCM
CO2 PERMEANCE (cm3(STP)/cm2/s/cmHg)
α(CO2/CH4)
10-3
10-4
10-5
400
300
200
100
20
40
60
80
100
120
140
160
HOURS

Figure 12

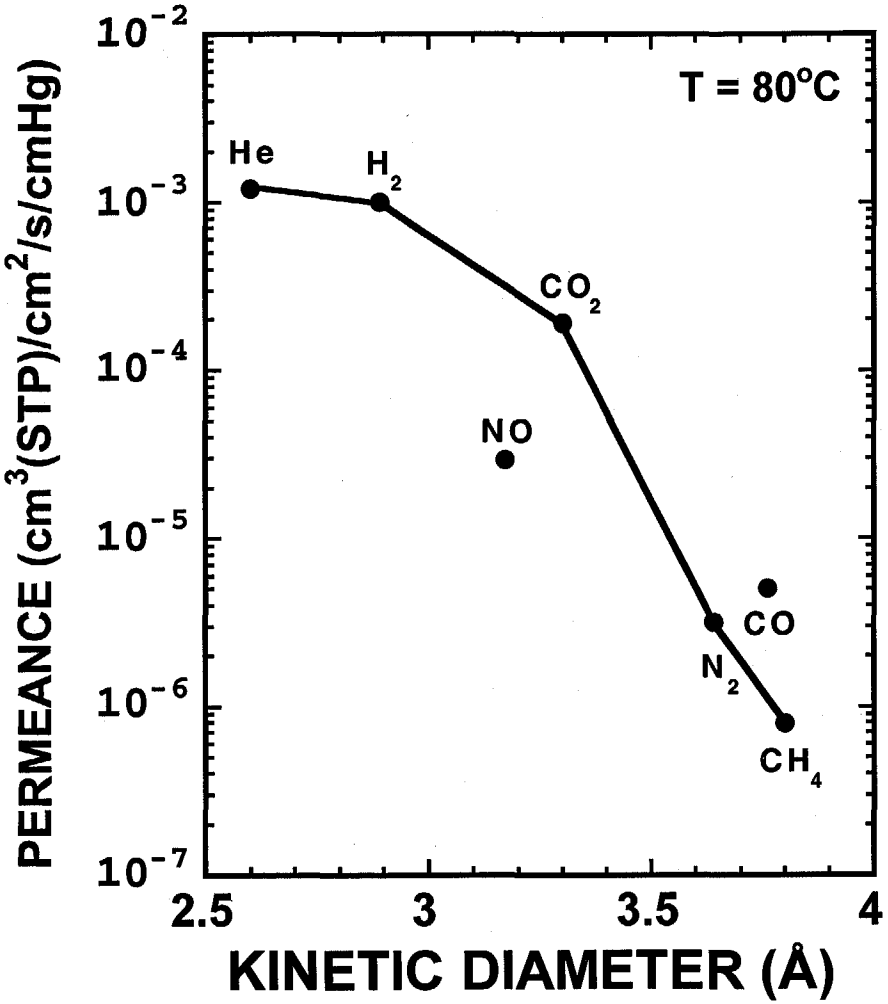

Gas Pair	*Ideal Separation Factor, α_I*
He/CH_4	1530
H_2/CH_4	1265
CO_2/N_2	60
CO_2/CH_4	240
NO/N_2	9.3

Figure 13

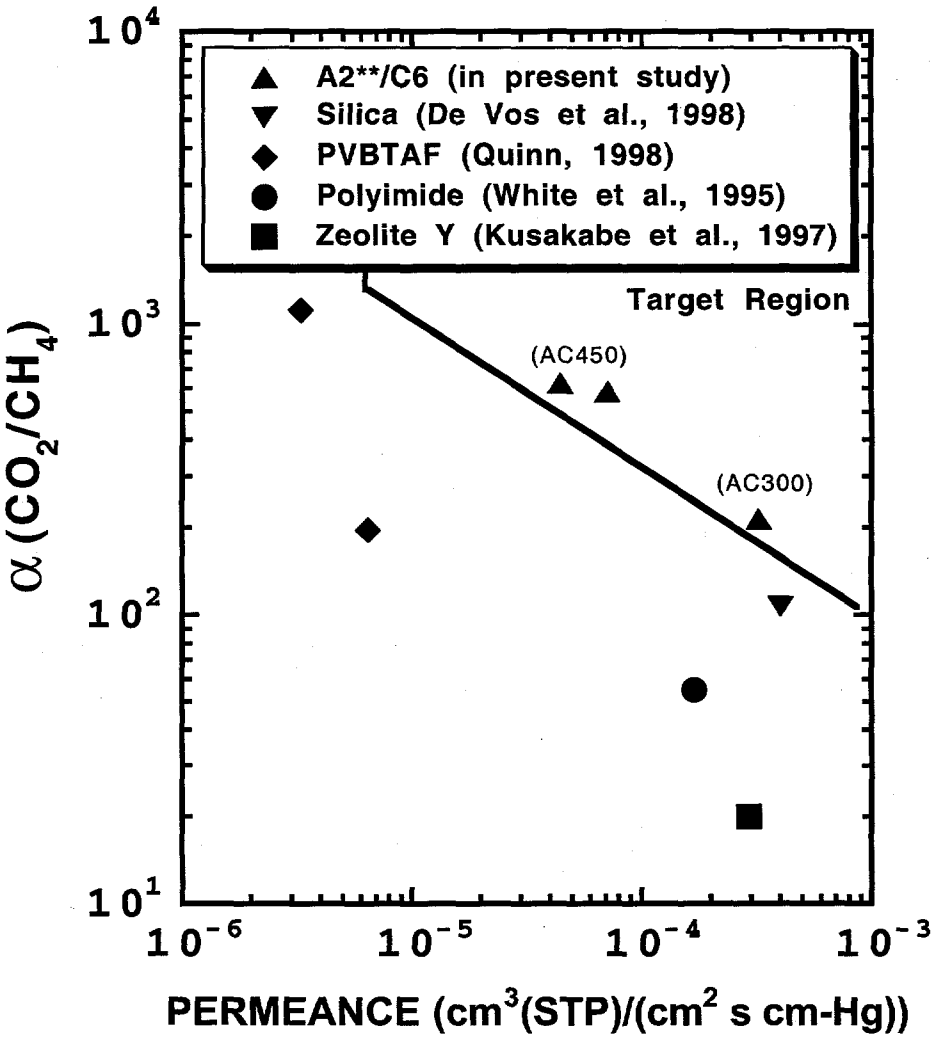
A2**/C6 (in present study)
Silica (De Vos et al., 1998)
PVBTAF (Quinn, 1998)
Polyimide (White et al., 1995)
Zeolite Y (Kusakabe et al., 1997)
Target Region
(AC450)
(AC300)
10^4
10^3
10^2
10^1
α (CO2/CH4)
10^-6
10^-5
10^-4
10^-3
PERMEANCE (cm3(STP)/(cm2 s cm-Hg))